

Correlated Cryo Super-Resolution Light and Cryo-Electron Microscopy on Mammalian Cells Expressing the Fluorescent Protein rsEGFP2

Maarten W. Tuijtel, Abraham J. Koster, Frank G. A. Faas,* and Thomas H. Sharp*

Super-resolution light microscopy (SRM) enables imaging of biomolecules within cells with nanometer precision. Cryo-fixation by vitrification offers optimal structure preservation of biological specimens and permits sequential cryo electron microscopy (cryoEM) on the same sample, but is rarely used for SRM due to various technical challenges and the lack of fluorophores developed for vitrified conditions. Here, a protocol to perform correlated cryoSRM and cryoEM on intact mammalian cells using fluorescent proteins and commercially available equipment is described. After cell culture and sample preparation by plunge-freezing, cryoSRM is performed using the reversibly photoswitchable fluorescent protein rsEGFP2. Next, a super-resolved image is reconstructed to guide cryoEM imaging to the feature of interest. Finally, the cryoSRM and cryoEM images are correlated to combine information from both imaging modalities. Using this protocol, a localization precision of 30 nm for cryoSRM is routinely achieved. No impediments to successive cryoEM imaging are detected, and the protocol is compatible with a variety of cryoEM techniques. When the optical set-up and analysis pipeline is established, the total duration of the protocol for experienced cryoEM users is 3 days, not including cell culture.

1. Introduction


Correlative light and electron microscopy (CLEM) combines data from fluorescence microscopy (FM) and electron microscopy (EM), two highly-complementary techniques, to image biological specimens.^[1–5] Biological samples are typically prepared for CLEM using chemical fixatives such as paraformaldehyde, which are known to introduce artefacts.^[6,7] In contrast, nonchemical vitrification, i.e., cryo-fixation, enables investigation of biological samples in an unperturbed, near-native state,^[8] and allows cryoCLEM to be utilized.^[9–13] Generally, (cryo)FM

is used to locate regions of interest, such as the location of labeled biomolecules, exploiting the large field of view provided by (cryo)FM. Alternatively, live-cell fluorescence microscopy can be performed prior to (cryo)fixation, to add temporal information to the sample.^[14–18] High-resolution information, such as the surrounding cellular ultrastructure, is not visible by (cryo)FM but can be provided by successive (cryo)EM investigation. In addition to the superior sample preservation, and in contrast to conventional “room-temperature” (RT-)CLEM, sample preparation methods for cryoCLEM are directly compatible with both imaging modalities and no intermediate processing steps that are known to perturb or damage the sample are necessary.^[19] However, the resolution gap between cryoFM and cryoEM is higher than that of RT-CLEM; the optical resolution of cryoFM is considerably lower than that achievable with RT-FM due to the long working-distance objective lenses

with a lower numerical aperture (NA),^[20] limiting the resolution of cryoFM to roughly 400 nm, while cryoEM can achieve sub-nanometer resolution.^[21] This resolution gap hinders accurate correlation, and hence interpretability, of cryoCLEM.^[22,23]

The resolution of FM can be improved by an order of magnitude by utilizing super-resolution microscopy (SRM).^[24,25] SRM includes techniques such as structured illumination microscopy,^[26,27] stimulated emission depletion microscopy (STED),^[28] reversible saturable optical fluorescence transitions (RESOLFT),^[29,30] and single-molecule localization microscopy (SMLM). SMLM encompasses methods such as photoactivated localization microscopy (PALM),^[31] fluorescence PALM,^[32] stochastic optical reconstruction microscopy,^[33] and ground state depletion microscopy followed by individual molecule return.^[34] This protocol describes cryoSMLM, which achieves super-resolution by imaging stochastically isolated individual fluorophores, such that their precise position can be determined with sub-pixel precision by fitting a model of the point spread function. By repeating the process of imaging different individual fluorophores and precise localization, a super-resolved image can be reconstructed by combining the localizations found in all images. SMLM has been successfully adapted for various RT-CLEM workflows,^[35–38] and extended to cryoCLEM.^[22,23,39,40] We recently described super-resolution cryoCLEM (SR-cryoCLEM)

M. W. Tuijtel,^[†] Prof. A. J. Koster, Dr. F. G. A. Faas, Dr. T. H. Sharp
Section Electron Microscopy
Department of Cell and Chemical Biology
Leiden University Medical Center
2300 RC Leiden, The Netherlands
E-mail: F.G.A.Faas@lumc.nl; T.Sharp@lumc.nl

 The ORCID identification number(s) for the author(s) of this article can be found under <https://doi.org/10.1002/smt.d.201900425>.

^[†]Present address: Wellcome Trust Centre for Cell Biology, University of Edinburgh, Michael Swann Building, Max Born Crescent, Edinburgh EH9 3BF, UK

DOI: 10.1002/smt.d.201900425

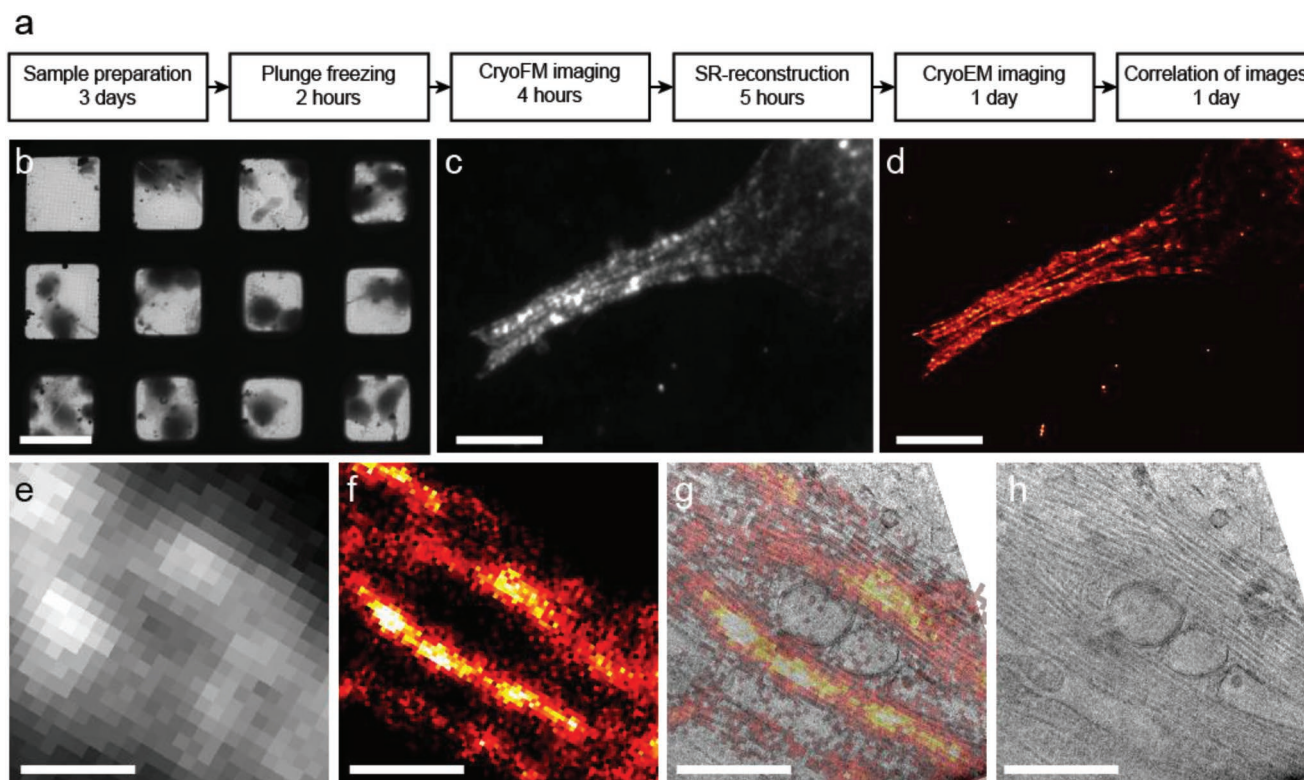


Figure 1. Overview of the protocol. a) Flow chart of the major steps of the protocol with the typical time scale required indicated for that step. Note that many steps do not require constant user interaction. For a detailed overview, see Figure S1 in the Supporting Information. b) CryoEM image of vitrified U2OS cells on an EM grid. c) CryoFM image of a U2OS cell transfected with rsEGFP-MAP2. d) CryoSRM image of the same area shown in (c). Separate microtubule bundles can clearly be distinguished, whereas this is not possible in the cryoFM image. e) Correlated cryoFM image of several bundles of microtubules inside a U2OS cell. f) Correlated and reconstructed cryoSRM image of the same region as shown in (e). g) CryoSRM image overlaid with a slice of a cryo-tomogram of the same region as shown in (e) and (f). h) The tomographic slice of the same region shown in (g), showing microtubules surrounding several liposomes. Scale bars: 100 μm in (b), 10 μm in (c) and (d), and 1 μm in (e–h).

on biological samples using genetically encoded fluorescent proteins and readily available equipment.^[23] In the protocol described herein, we explain how we perform SR-cryoCLEM on vitrified intact mammalian cells, without compromising successive cryoEM imaging (Figure 1 and Supporting Information).

2. Protocol Overview

An overview of the protocol steps and time requirements is shown in Figure 1a and Figure S1 in the Supporting Information. After performing initial calibrations (Calibration Protocols #1 and #2 in the Supporting Information), this protocol takes 6 days to complete, including 3 days of cell culture and transfection to express the fluorescently labeled proteins (see Culture and transfect U2OS cells on EM grids in the Supporting Information). Vitrification is performed using plunge freezing (see Sample preparation by plunge-freezing grids in the Supporting Information), after which imaging (described in the sections Cryo super-resolution acquisition, Analysis and reconstruction of super-resolution data, Create overview of FM positions, and Cryo-transmission electron microscope image acquisition in the Supporting Information) takes 2 days. Finally, image correlation can be performed in 1 day (see Correlate cryoFM, cryoSRM, and cryoEM images in the Supporting Information).

There are many “pause points” throughout the protocol that are noted in the Supporting Information which allow samples to be stored in liquid nitrogen (LN2) for extended periods of time. A complete list of materials and reagents required to perform this protocol is also provided (Supporting Information). The typical results expected after performing this protocol are shown in Figure 1; comparing Figure 1e,f shows the improvement in resolution from cryoFM (Figure 1e) to cryoSMLM (Figure 1f), especially when correlated with a cryoEM image.

To achieve this resolution improvement, several challenges must be addressed when adapting SRM for cryosamples.^[20,41] Vitrified samples must be kept below 133 K at all times to avoid devitrification and crystallization of the vitreous water in the sample, which causes severe structural damage to the near-native sample and impedes subsequent cryoEM imaging.^[20,22,23,39] Also, many SRM techniques depend on nonlinear effects of fluorophores that become apparent when illuminated with high intensity light.^[42] However, intense illumination can cause devitrification.^[22,23,39] We have systematically determined the illumination intensity that is sufficient to perform cryoSRM without any sample devitrification (Calibration Protocol #2 in the Supporting Information), and without using cryoprotectants to maintain the native environment of the biological specimens.^[23] We have previously described that photon-induced devitrification starts in the center of the grid

squares,^[23] indicating that other grid types or support films may allow a higher illumination intensity (see also Note 3 in the Supporting Information).

Another consideration is the complexity of the optical set-up: STED/RESOLFT requires a scanning microscopy system, with an elaborate optical set-up to achieve the desired illumination pattern: SMLM typically uses a standard wide-field set-up, which is less expensive than STED microscopes, and does not require precise alignment of illumination schemes to stimulate photon emission depletion (Note 1 in the Supporting Information).

It is undesirable to permeabilize cellular membranes or use external labeling strategies in order to maintain the near-native conditions of the cryo-preserved sample. Genetic labels, such as reversibly photoswitchable fluorescent proteins (RSFPs), can be expressed within the sample, thereby removing the need for invasive labeling steps. Furthermore, SMLM can be performed by switching RSFPs on and off.^[22,23,39,43–45] However, the behavior of RSFPs in a vitreous surrounding and at low temperature (77 K) is different than at RT,^[22,23,39,45–48] and the mechanism that underlies the switching under these conditions is poorly understood.^[47–49] Indeed, we have shown similar switching behavior of all fluorescent proteins (FPs) tested so far under vitreous conditions, suggesting that any FP can be used to perform SR-cryoCLEM.^[23] RSFPs appear to retain their photoactivatability at low temperatures, although switching kinetics are much slower compared to RT.^[23,39,45,47,48] Despite this, several (RS)FPs have been successfully employed to perform cryoSRM.^[22,23,39,45,46] Here, we have used rsEGFP2,^[50] which showed favorable characteristics when vitrified and imaged at low temperatures, including intensity, background, and deactivation rate,^[23] although other (RS)FPs can also be used.^[22,23,39] In order to overcome the slower kinetics and subsequent higher background of RSFPs at low temperatures, some adaptations to standard RT-SMLM imaging protocols were made. First, prior to SMLM imaging, the majority of probes have to be put in their off-state, a process that takes seconds at RT, but can take up to 20 min per imaging position when imaging cryosamples.^[23] However, we have discovered that RSFPs can be deactivated prior to vitrification, after which their off-state is retained for prolonged periods of time, which significantly reduces imaging times.^[23] Furthermore, during SMLM imaging, many cycles of activation and imaging are repeated and processed to reconstruct a super-resolved image. Instead of waiting until all activated RSFPs have been completely deactivated, which takes up to 20 min due to the slower kinetics at $-196\text{ }^{\circ}\text{C}$, we developed an image-differencing method to detect only newly activated RSFPs in each imaging cycle.^[23]

Lastly, cryostages generally experience more drift compared to RT stages, due to instabilities caused by the large temperature gradients between the LN₂ cooled stage and the ambient surroundings.^[20] Various methods have been developed to mitigate the drift, for instance by adapting existing cryostages with an active feedback system that measures and corrects movements during imaging,^[22,39,51] or by using fiducial beads to perform image registration after acquisition.^[22,23] We correct for lateral drift after acquisition by registering the images based on fiducial beads or the residual fluorescence from the sample itself, which allows the commercially available Linkam cryostage to

be used without further adjustments. To reduce drift effects, instead of a single, long exposure, we used relatively fast and short camera acquisitions that are subsequently aligned (Note 2 in the Supporting Information). Drift in the axial direction (along the optical axis) manifests as defocusing and cannot be corrected after acquisition. This was mitigated during imaging by refocusing when the image drifted out of focus. We also found that the slower deactivation of fluorophores reduced the rate of SR-image acquisition at least tenfold.^[23] To counter this, we used the aforementioned image-differencing method, which greatly accelerates data acquisition (Note 2 in the Supporting Information).

To facilitate the use of this Protocol and data analysis when reconstructing the super-resolution image, we have included a Matlab-script accompanied by a manual and test data (Supporting Appendix).

3. Applications and Future Perspectives

In this protocol, we describe how to perform SR-cryoCLEM on mammalian cells transfected with MAP2-rsEGFP that localizes to microtubules (Figure 1 and Supporting Information). We routinely perform this protocol and achieve a localization precision of 30 nm, with a success rate of $\approx 83\%$.^[23]

Localizing individual or rare proteins and transient biomolecular complexes in situ using cryoEM is difficult due to the crowded cellular landscape that is visible by cryoEM. Currently, proteins are identified by, e.g., immunolabeling using gold beads,^[52,53] or tagged with proteins that accumulate heavy metals to become electron dense.^[54,55] However, these are not optimal, with generally a poor binding efficiency and difficulties with intracellular delivery of both heavy metals and (immuno) labeling agents.^[56] The SR-cryoCLEM methodology described herein could yield the means to precisely localize and identify labeled proteins in the crowded cellular landscape provided by cryoEM using genetic FP tags, such as rsEGFP2, to replace electron-dense markers.

This protocol is compatible with cryoEM techniques in general, such as single-particle analysis and 3D cryo-electron tomography,^[23] making this technique broadly applicable as a tool for in situ structural biology. Furthermore, the recent development of cryo focused ion beam (FIB) milling as a method to section thick biological specimens, such as the nuclei of cells, has opened up a range of samples and biological questions in cellular regions that were previously too thick for cryoEM investigation.^[57,58] We anticipate a need for targeted FIB-milling, so that relatively rare events or proteins can first be precisely located using cryoSRM, after which those regions can be thinned using FIB milling and finally high-resolution cryo-electron tomography can be performed to collect structural data.^[59,60] Additionally, we envision that cryoSRM can be an alternative to RT-SRM even without further cryoEM investigation, so that artefacts caused by chemical fixation can be avoided through fixation by vitrification.^[24,61–63]

This protocol aims to make cryoSRM and SR-cryoCLEM routine and straightforward. However, the resolution in the axial (z -)direction remains diffraction-limited in this protocol, typically $\approx 1.8\text{ }\mu\text{m}$ when using objective lenses suitable for

cryoFM. Samples for cryoEM must be thin enough to allow transmission of electrons, typically less than 500 nm and more usually less than 200 nm, which improves the axial resolution. The localization precision within thick vitrified samples, such as those prepared for cryoFIB milling, remains limited. The axial resolution could be improved by, e.g., placing a cylindrical lens in the optical system so changes in location can be estimated by measuring the astigmatism of the detected single-molecule signals.^[39,64] Alternatively, the resolution of cryoSRM could be further improved by enabling objective lenses with a higher NA, for instance by utilizing immersion lenses.^[65–67] Nevertheless, by employing the reduced photobleaching characteristics of FPs inherent with low temperature imaging,^[13,68–70] localization accuracies in the sub-nm range have been achieved.^[68,71]

Supporting Information

Supporting Information is available from the Wiley Online Library or from the author.

Acknowledgements

M.W.T. and F.G.A.F. developed the optical set-up and acquisition software. M.W.T., A.J.K., F.G.A.F., and T.H.S. designed the experiments. M.W.T. and T.H.S. acquired and analyzed cryo-electron tomography data. M.W.T. performed the experiments, acquired and analyzed all data, and designed the data analysis workflow. M.W.T. and T.H.S. wrote the manuscript. All authors commented on the manuscript. This research was supported by grants from the Netherlands Organization for Scientific Research Stichting Technologische Wetenschappen Perspectief Grant Microscopy Valley (grant number STW12713 to A.J.K.) and the European Research Council (grant no. 759517 to T.H.S.). The authors gratefully acknowledge Frauke Liebelt for assistance with mammalian cell culture, and Georg Wolff, Willem Noteborn, and Roman Koning for testing and commenting on the protocol.

Conflict of Interest

The authors declare no conflict of interest.

Keywords

correlative light and electron microscopy, cryoEM, cryo-fluorescence microscopy, super-resolution microscopy

Received: June 5, 2019

Published online:

- [1] D. M. van Elsland, E. Bos, W. de Boer, H. S. Overkleeft, A. J. Koster, S. I. van Kasteren, *Chem. Sci.* **2016**, *7*, 752.
- [2] W. Kukulska, M. Schorb, S. Welsch, A. Picco, M. Kaksonen, J. A. Briggs, *J. Cell Biol.* **2011**, *192*, 111.
- [3] L. Collinson, P. Verkade, *J. Chem. Biol.* **2015**, *8*, 127.
- [4] T. Müller-Reichert, P. Verkade, *Correlative Light and Electron Microscopy II*, Vol. 124, Academic Press, San Diego, CA **2014**.
- [5] R. I. Koning, K. Celler, J. Willemse, E. Bos, G. P. van Wezel, A. J. Koster, in *Methods in Cell Biology*, Vol. 124, (Ed: T. Müller-Reichert, P. Verkade), Elsevier, New York **2014**, pp. 217–239.

- [6] I. Hurbain, M. Sachse, *Biol. Cell* **2011**, *103*, 405.
- [7] C. Bleck, A. Merz, M. Gutierrez, P. Walther, J. Dubochet, B. Zuber, G. Griffiths, *J. Microsc.* **2010**, *237*, 23.
- [8] L. Mielanczyk, N. Matysiak, M. Michalski, R. Buldak, R. Wojnicz, *Folia Histochem. Cytobiol.* **2014**, *52*, 1.
- [9] L. F. van Driel, J. A. Valentijn, K. M. Valentijn, R. I. Koning, A. J. Koster, *Eur. J. Cell Biol.* **2009**, *88*, 669.
- [10] A. Sartori, R. Gatz, F. Beck, A. Rigort, W. Baumeister, J. M. Plitzko, *J. Struct. Biol.* **2007**, *160*, 135.
- [11] J. M. Plitzko, A. Rigort, A. Leis, *Curr. Opin. Biotechnol.* **2009**, *20*, 83.
- [12] M. Schorb, L. Gaechter, O. Avinoam, F. Sieckmann, M. Clarke, C. Bebeacua, Y. S. Bykov, A. F.-P. Sonnen, R. Lihl, J. A. Briggs, *J. Struct. Biol.* **2017**, *197*, 83.
- [13] C. L. Schwartz, V. I. Sarbash, F. I. Ataullakhanov, J. R. McIntosh, D. Nicastro, *J. Microsc.* **2007**, *227*, 98.
- [14] J. Fermie, N. Liv, C. ten Brink, E. G. van Donselaar, W. H. Müller, N. L. Schieber, Y. Schwab, H. C. Gerritsen, J. Klumperman, *Traffic* **2018**, *19*, 354.
- [15] G. M. Gaietta, B. N. Giepmans, T. J. Deerinck, W. B. Smith, L. Ngan, J. Llopis, S. R. Adams, R. Y. Tsien, M. H. Ellisman, *Proc. Natl. Acad. Sci. USA* **2006**, *103*, 17777.
- [16] R. I. Koning, F. G. Faas, M. Boonekamp, B. de Visser, J. Janse, J. C. Wiegant, A. de Breij, J. Willemse, P. H. Nibbering, H. J. Tanke, *Ultramicroscopy* **2014**, *143*, 67.
- [17] P. Verkade, *J. Microsc.* **2008**, *230*, 317.
- [18] M. Fuest, G. Nocera, M. Modena, D. Riedel, Y. Mejia, T. Burg, *J. Microsc.* **2018**, *272*, 87.
- [19] U. Schnell, F. Dijk, K. A. Sjollem, B. N. Giepmans, *Nat. Methods* **2012**, *9*, 152.
- [20] G. Wolff, C. Hagen, K. Grünwald, R. Kaufmann, *Biol. Cell* **2016**, *108*, 245.
- [21] W. Kühlbrandt, *Science* **2014**, *343*, 1443.
- [22] Y.-W. Chang, S. Chen, E. I. Tocheva, A. Treuner-Lange, S. Löbach, L. Søgaard-Andersen, G. J. Jensen, *Nat. Methods* **2014**, *11*, 737.
- [23] M. W. Tuijtel, A. J. Koster, S. Jakobs, F. G. A. Faas, T. H. Sharp, *Sci. Rep.* **2019**, *9*, 1369.
- [24] S. W. Hell, S. J. Sahl, M. Bates, X. Zhuang, R. Heintzmann, M. J. Booth, J. Bewersdorf, G. Shtengel, H. Hess, P. Tinnefeld, *J. Phys. D: Appl. Phys.* **2015**, *48*, 443001.
- [25] B. Huang, M. Bates, X. Zhuang, *Annu. Rev. Biochem.* **2009**, *78*, 993.
- [26] M. G. Gustafsson, *J. Microsc.* **2000**, *198*, 82.
- [27] R. Heintzmann, C. Cremer, *Proc. SPIE* **1999**, *3568*, 15.
- [28] S. W. Hell, J. Wichmann, *Opt. Lett.* **1994**, *19*, 780.
- [29] M. Hofmann, C. Eggeling, S. Jakobs, S. W. Hell, *Proc. Natl. Acad. Sci. USA* **2005**, *102*, 17565.
- [30] S. W. Hell, *Nat. Biotechnol.* **2003**, *21*, 1347.
- [31] E. Betzig, G. H. Patterson, R. Sougrat, O. W. Lindwasser, S. Olenych, J. S. Bonifacio, M. W. Davidson, J. Lippincott-Schwartz, H. F. Hess, *Science* **2006**, *313*, 1642.
- [32] S. T. Hess, T. P. Girirajan, M. D. Mason, *Biophys. J.* **2006**, *91*, 4258.
- [33] M. J. Rust, M. Bates, X. Zhuang, *Nat. Methods* **2006**, *3*, 793.
- [34] J. Fölling, M. Bossi, H. Bock, R. Medda, C. A. Wurm, B. Hein, S. Jakobs, C. Eggeling, S. W. Hell, *Nat. Methods* **2008**, *5*, 943.
- [35] E. Johnson, E. Seiradake, E. Y. Jones, I. Davis, K. Grünwald, R. Kaufmann, *Sci. Rep.* **2015**, *5*, 9583.
- [36] D. Kim, T. J. Deerinck, Y. M. Sigal, H. P. Babcock, M. H. Ellisman, X. Zhuang, *PLoS One* **2015**, *10*, e0124581.
- [37] S. Watanabe, A. Punge, G. Hollopeter, K. I. Willig, R. J. Hobson, M. W. Davis, S. W. Hell, E. M. Jorgensen, *Nat. Methods* **2011**, *8*, 80.
- [38] M. G. Paez-Segala, M. G. Sun, G. Shtengel, S. Viswanathan, M. A. Baird, J. J. Macklin, R. Patel, J. R. Allen, E. S. Howe, G. Piszczek, *Nat. Methods* **2015**, *12*, 215.
- [39] B. Liu, Y. Xue, W. Zhao, Y. Chen, C. Fan, L. Gu, Y. Zhang, X. Zhang, L. Sun, X. Huang, *Sci. Rep.* **2015**, *5*, 13017.

- [40] F. Moser, V. Pražák, V. Mordhorst, D. M. Andrade, L. A. Baker, C. Hagen, K. Grünewald, R. Kaufmann, *Proc. Natl. Acad. Sci. USA* **2019**, *116*, 4804.
- [41] R. Kaufmann, C. Hagen, K. Grünewald, *Curr. Opin. Chem. Biol.* **2014**, *20*, 86.
- [42] S. W. Hell, *Nat. Methods* **2009**, *6*, 24.
- [43] A. Egner, C. Geisler, C. Von Middendorff, H. Bock, D. Wenzel, R. Medda, M. Andresen, A. C. Stiel, S. Jakobs, C. Eggeling, *Biophys. J.* **2007**, *93*, 3285.
- [44] N. A. Jensen, J. G. Danzl, K. I. Willig, F. Lavoie-Cardinal, T. Brakemann, S. W. Hell, S. Jakobs, *ChemPhysChem* **2014**, *15*, 756.
- [45] P. D. Dahlberg, A. M. Sartor, J. Wang, S. Saurabh, L. Shapiro, W. E. Moerner, *J. Am. Chem. Soc.* **2018**, *140*, 12310.
- [46] R. Kaufmann, P. Schellenberger, E. Seiradake, I. M. Dobbie, E. Y. Jones, I. Davis, C. Hagen, K. Grünewald, *Nano Lett.* **2014**, *14*, 4171.
- [47] A. R. Faro, V. Adam, P. Carpentier, C. Darnault, D. Bourgeois, E. de Rosny, *Photochem. Photobiol. Sci.* **2010**, *9*, 254.
- [48] A. Regis Faro, P. Carpentier, G. Jonasson, G. Pompidor, D. Arcizet, I. Demachy, D. Bourgeois, *J. Am. Chem. Soc.* **2011**, *133*, 16362.
- [49] M. Andresen, A. C. Stiel, S. Trowitzsch, G. Weber, C. Eggeling, M. C. Wahl, S. W. Hell, S. Jakobs, *Proc. Natl. Acad. Sci. USA* **2007**, *104*, 13005.
- [50] T. Grotjohann, I. Testa, M. Reuss, T. Brakemann, C. Eggeling, S. W. Hell, S. Jakobs, *eLife* **2012**, *1*, e00248.
- [51] X. Xu, Y. Xue, B. Tian, F. Feng, L. Gu, W. Li, W. Ji, T. Xu, *Sci. China Life Sci.* **2018**, *61*, 1312.
- [52] G. Cardone, D. C. Winkler, B. L. Trus, N. Cheng, J. E. Heuser, W. W. Newcomb, J. C. Brown, A. C. Steven, *Virology* **2007**, *361*, 426.
- [53] Y. Turgay, M. Eibauer, A. E. Goldman, T. Shimi, M. Khayat, K. Ben-Harush, A. Dubrovsky-Gaup, K. T. Sapra, R. D. Goldman, O. Medalia, *Nature* **2017**, *543*, 261.
- [54] C. Bouchet-Marquis, M. Pagratis, R. Kirmse, A. Hoenger, *J. Struct. Biol.* **2012**, *177*, 119.
- [55] Q. Wang, C. P. Mercogliano, J. Löwe, *Structure* **2011**, *19*, 147.
- [56] T. Oda, M. Kikkawa, *J. Struct. Biol.* **2013**, *183*, 305.
- [57] J. Arnold, J. Mahamid, V. Lucic, A. de Marco, J.-J. Fernandez, T. Laugks, T. Mayer, A. A. Hyman, W. Baumeister, J. M. Plitzko, *Biophys. J.* **2016**, *110*, 860.
- [58] J. Mahamid, S. Pfeffer, M. Schaffer, E. Villa, R. Danev, L. K. Cuellar, F. Förster, A. A. Hyman, J. M. Plitzko, W. Baumeister, *Science* **2016**, *351*, 969.
- [59] Y. Fukuda, U. Laugks, V. Lučić, W. Baumeister, R. Danev, *J. Struct. Biol.* **2015**, *190*, 143.
- [60] L. Gan, G. J. Jensen, *Q. Rev. Biophys.* **2012**, *45*, 27.
- [61] D. R. Whelan, T. D. Bell, *Sci. Rep.* **2015**, *5*, 7924.
- [62] K. A. Tanaka, K. G. Suzuki, Y. M. Shirai, S. T. Shibutani, M. S. Miyahara, H. Tsuboi, M. Yahara, A. Yoshimura, S. Mayor, T. K. Fujiwara, *Nat. Methods* **2010**, *7*, 865.
- [63] P. Annibale, M. Scarselli, M. Greco, A. Radenovic, *Opt. Nanosc.* **2012**, *1*, 9.
- [64] B. Huang, W. Wang, M. Bates, X. Zhuang, *Science* **2008**, *319*, 810.
- [65] M. Metzger, A. Konrad, S. Skandary, I. Ashraf, A. J. Meixner, M. Brecht, *Opt. Express* **2016**, *24*, 13023.
- [66] M. Le Gros, G. McDermott, M. Uchida, C. Knoechel, C. Larabell, *J. Microsc.* **2009**, *235*, 1.
- [67] R. Faoro, M. Bassu, Y. X. Mejia, T. Stephan, N. Dudani, C. Boeker, S. Jakobs, T. P. Burg, *Proc. Natl. Acad. Sci. USA* **2018**, *115*, 1204.
- [68] S. Weisenburger, B. Jing, D. Hänni, L. Reymond, B. Schuler, A. Renn, V. Sandoghdar, *ChemPhysChem* **2014**, *15*, 763.
- [69] W. Moerner, M. Orrit, *Science* **1999**, *283*, 1670.
- [70] M. W. Tuijtel, A. A. Mulder, C. C. Posthuma, B. van der Hoeven, A. J. Koster, M. Barcena, F. G. A. Faas, T. H. Sharp, *Sci. Rep.* **2017**, *7*, 10442.
- [71] C. N. Hulleman, W. Li, I. Gregor, B. Rieger, J. Enderlein, *ChemPhysChem* **2018**, *19*, 1774.